Curling-like Bi$_2$WO$_6$ microdiscs with lamellar structure for enhanced gas-sensing properties

Zheng Lou, Jianan Deng, Lili Wang, Lijie Wang, Tong Zhang[*]

State Key Laboratory on Integrated Optoelectronics, College of Electronic Science and Engineering, Jilin University, Changchun 130012, PR China

ARTICLE INFO

ABSTRACT

Self-assembled curling-like Bi$_2$WO$_6$ microdiscs, consisting of closely packed nanosheets with thickness of 50 nm, have been successfully synthesized by a simple solvothermal route. This structure was characterized by field emission scanning electron microscopic (FESEM) and transmission electron microscopy (TEM). The results show that the Bi$_2$WO$_6$ samples are mostly microdiscs in shape and have an average side thickness of 500 nm. The time-dependent morphology of the Bi$_2$WO$_6$ samples has been investigated, and gas sensors based on these products were fabricated for ethanol detection. The sensor based on the curling-like Bi$_2$WO$_6$ nanostructures shows much better sensing properties than other Bi$_2$WO$_6$ structures. The response of the curling-like Bi$_2$WO$_6$ sensor to 100 ppm ethanol is about 11.9 with the response time of 1 s. The dramatic improvement in sensing properties of the present curling-like Bi$_2$WO$_6$ sensor may be attributed to the unique structures, the good crystallization and large surface area.

1. Introduction

It is well known that the physical and chemical properties of most materials are strongly dependent on their shape and structure [1,2]. In particular, the alignment of nanostructure building blocks (nanoparticles, nanorods, and nanosheets) into three-dimensional superstructures received great attentions, owing to their potential applications in electronic, magnetic, optoelectronic, catalytic, sensing and biomedical fields [3–7]. To date, intensive studies have been carried out on the synthesis of hierarchical binary oxide nanostructures as well as the exploration of their novel properties, for example, ZnO, NiO, In$_2$O$_3$, SnO$_2$, and WO$_3$ [3,8–12]. However, in comparison with simple binary oxides, there are still very few studies concerning multicomponent oxides nanostructures, though multicomponent oxides have more freedom to tune the chemical and physical properties of materials by altering the compositions and more defects which are good for the photocatalytic and gas sensors [13].

Bismuth tungstate (Bi$_2$WO$_6$), as one kind of multicomponent metal oxide compounds with wide-bandgap (E_g = 2.69 eV) [14], has received great interest over the past few years because of its potential applications in photoluminescence, microwave, optical fibers, catalysts, magnetic devices, and chemical sensors [15–17]. In recent years, stimulated by the promising applications

of Bi$_2$WO$_6$ and the novel properties of nanomaterials, much effort has been made to synthesize Bi$_2$WO$_6$ with various morphologies, such as nanoparticles, nanoplates, nanospheres, and nanosheets [14,18,19]. Significantly, Luo [20] and Wang [21] groups have reported the preparation of Bi$_2$WO$_6$ hollow spheres and hierarchical structures by the typical hydrothermal process and improved their visible-light-driven photocatalytic activities. These works revealed that different shape, size and structure of Bi$_2$WO$_6$ materials could realize different physicochemical properties, which might be beneficial for sensing application. Very recently, Chen and coworkers [22] reported on the synthesis of unusual Aurivillius type Bi$_2$WO$_6$ hierarchical structures by the "Doctor Blade" method, which were found to exhibit unusual humidity sensing properties. This has triggered an immense research interest in the synthesis of Bi$_2$WO$_6$ structures and in the investigation of the corresponding relations between sensing activity and morphology.

To enrich the research in this area, herein, we demonstrate a facile solvothermal route for controllable synthesis of curling-like Bi$_2$WO$_6$ microdiscs in the presence of sodium citrate in a glycol/H$_2$O two-phase system without any templates. By tuning appropriate solvothermal reaction times, Bi$_2$WO$_6$ with different shapes, grain sizes, and structures can be controllably synthesized. Correspondingly, the obtained nanostructures have been fabricated into gas sensors and used to detect some gases such as ethanol. The results show that the gas sensors based on curling-like Bi$_2$WO$_6$ microdiscs exhibit high response, fast response time, and good selectivity for ethanol, which should be attributed to the surface structure of the nanocrystals and good crystallization.

* Corresponding author. Tel.: +86 431 85168385; fax: +86 431 85168270.
  E-mail address: zhangtong@jlu.edu.cn (T. Zhang).

Table 1
Structural parameters of Bi_2WO_6 samples from different reaction times.

Sample no.	React time (min)	Size (μm)	S_{BET} (m^2 g^{-1})	Morphology
S-1	0	~0.02	4.0	Nanoparticles
S-2	10	~1.5	7.3	Nanoparticles/sheets
S-3	30	~1.5	16.5	Disc-like structures
S-4	60	~1.5	28.7	Curing-like microdiscs

2. Experimental

2.1. Synthesis of curling-like Bi_2WO_6 microdiscs

All chemical reagents in this work were purchased from the Shanghai Chemical Company. They were of analytical grade and used without further purification. In a typical procedure, 0.243 g of $Bi(NO_3)_3 \cdot 5H_2O$ and 0.1 g of sodium citrate were added into 30 mL of glycol/H_2O mixed solution with a volume ratio of 1:1 to form the metal–citrate complex. After vigorous stirring for 10 min, 0.33 g of $Na_2WO_4 \cdot 2H_2O$ was introduced into above solution. After further agitation for 5 min, the solution was poured into a stainless steel autoclave with a Teflon liner of 50 mL capacity and heated at 180 °C for 60 min. After the autoclave had cooled to room temperature, the products were separated centrifugally and washed with ultra-pure water and absolute ethanol several times. Then, the products were dried under vacuum at 80 °C for 6 h. Table 1 showed different detailed parameters of curling-like Bi_2WO_6 microdiscs and other Bi_2WO_6 samples.

2.2. Characterizations

The product was characterized by X-ray diffraction (XRD) using a Rigaku D/Max-2550 diffractometer with Cu Kα radiation ($\lambda = 0.15418$ nm, 40 kV, 350 mA) in the range of 20–80° (2θ) at a scanning rate of 6° min^{-1}. The morphologies characteristic of samples were obtained on a XL 30 ESEM FEG field emission scanning electron microscope (FESEM). TEM and HRTEM images were recorded with a Tecnai G^2 20S-Twin transmission electron microscope operating at an accelerating voltage of 120 and 200 kV, respectively. The energy dispersive X-ray (EDX) analysis was also performed during transmission electron microscope (TEM) measurements. Specific surface areas were computed from the results of N_2 physisorption at 77 K (model: BECKMAN SA3100 COULTER) using the BET (Brunauer–Emmett–Teller) formalism.

2.3. Fabrication and measurement of gas sensors

The as-synthesized sample was mixed with deionized water in a weight ratio of 4:1 to form a paste. The paste to form about 600 μm sensing film was coated on a ceramic tube on which a pair of gold electrodes was previously printed. The structure of the sensor is shown in Fig. 1. Gas-sensing measurements were made in a static system and different concentrations of ethanol were introduced to the testing chamber (1 L) by an injection. The details of the sensor fabrication are similar to those reported in the literature [8].

The electrical properties of the sensor were measured by the CGS intelligent test system (China). The response ($S = R_a/R_g$) of the sensor was defined as the ratio of sensor resistance in dry air (R_a) to that in a target gas (R_g) between 240 and 360 °C. The time taken by the resistor to range from R_a to $R_a - 90\% (R_a - R_g)$ is defined as the response time, when the sensor is exposed to the target gas. The time taken by the resistor to range from R_g to $R_g + 90\% (R_a - R_g)$ is defined as the recovery time, when the sensor is departed from the target gas.
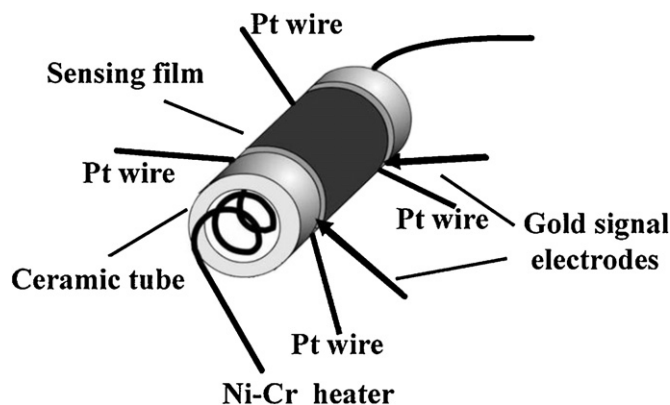

Fig. 1. Schematic structure of the gas sensor.

3. Results and discussion

3.1. Structural and morphological characteristics

The XRD pattern of the as-prepared product is shown in Fig. 2. It is shown that all the diffraction peaks for the as-synthesized product can be indexed as orthorhombic bismuth tungstate (Bi_2WO_6), having orthorhombic structure (JCPDS No. 73-1126). No phases corresponding to impurities are detected in the XRD pattern.

The morphologies of the as-prepared Bi_2WO_6 products with different reaction times were investigated in detail by FESEM, which are shown in Fig. 3. Before reaction-treatment, it can be observed that the sample consists of some irregular nanoparticles agglomerates, as shown in a panoramic image (S-1, Fig. 3a). When the solvothermal time is 10 min (S-2), a small amount of sheet-like structures with size of about 1.5–2.0 μm slowly formed, and the irregular particles coexisted in the system, as seen from Fig. 3b. Increasing the solvothermal time to 30 min (S-3), oriented aggregation happened and many nanoparticles and nanosheets aggregated into analogous disc-like lamellar structures (Fig. 3c). Interestingly, when the solvothermal time is increased to 60 min (S-4), many disc-like lamellar structures with a few peaks appeared. The typical curling-like Bi_2WO_6 microdiscs are formed (Fig. 3d). More details can be observed in the inset of Fig. 3d, which demonstrates that the discs with an average side thickness of 500 nm are formed multi-layered structures by many nanosheets. This hierarchical network
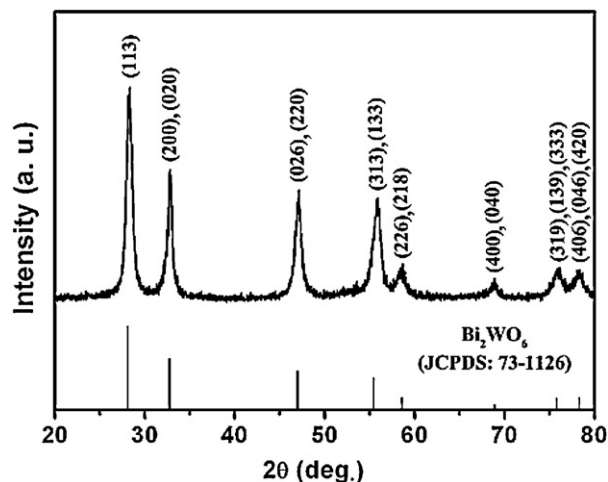

Fig. 2. XRD patterns of curling-like Bi_2WO_6 microdiscs prepared by a hydrothermal method with a reaction time of 60 min.
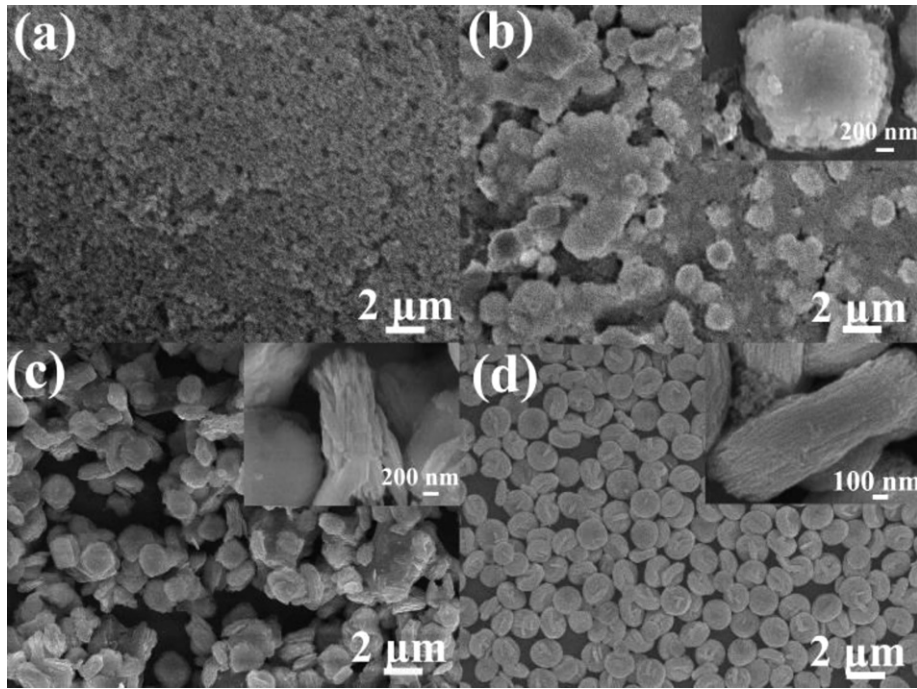
Fig. 3. FESEM images of the products obtained with different reaction times: (a) 0 min, (b) 10 min, (c) 30 min and (d) 60 min.

is believed to be favorable for gas sensors, which can facilitate the inward and outward gas diffusion.

Further investigation was carried out by TEM and HRTEM to reveal the organization of such self-assembled complex structures. A TEM image of typical S-4 is shown in Fig. 4a. The diameter of the S-4 is about 1.5 μm (Fig. 4b), which agrees well with the FESEM images (Fig. 3d). Combined with the observed concaves in FESEM, it is reasonable to conclude that the central section of the microdiscs

is thinner than the edges of such structures. Fig. 4c presents the side of an individual microdisc, and we can see that the convexity part is formed by the nanosheets. Fig. 4d and e are the HRTEM images taken from the sections 1 (Fig. 4b) and 2 (Fig. 4c) of the microdiscs. From Fig. 4d, the lattice interplanar spacing is measured to be 0.274 nm, corresponding to the (2 0 0) plane of orthorhombic Bi_2WO_6. As can be seen from Fig. 4e, the d spacings are 0.272 and 0.193 nm, which agrees well with the lattice spacing of (0 2 0) and
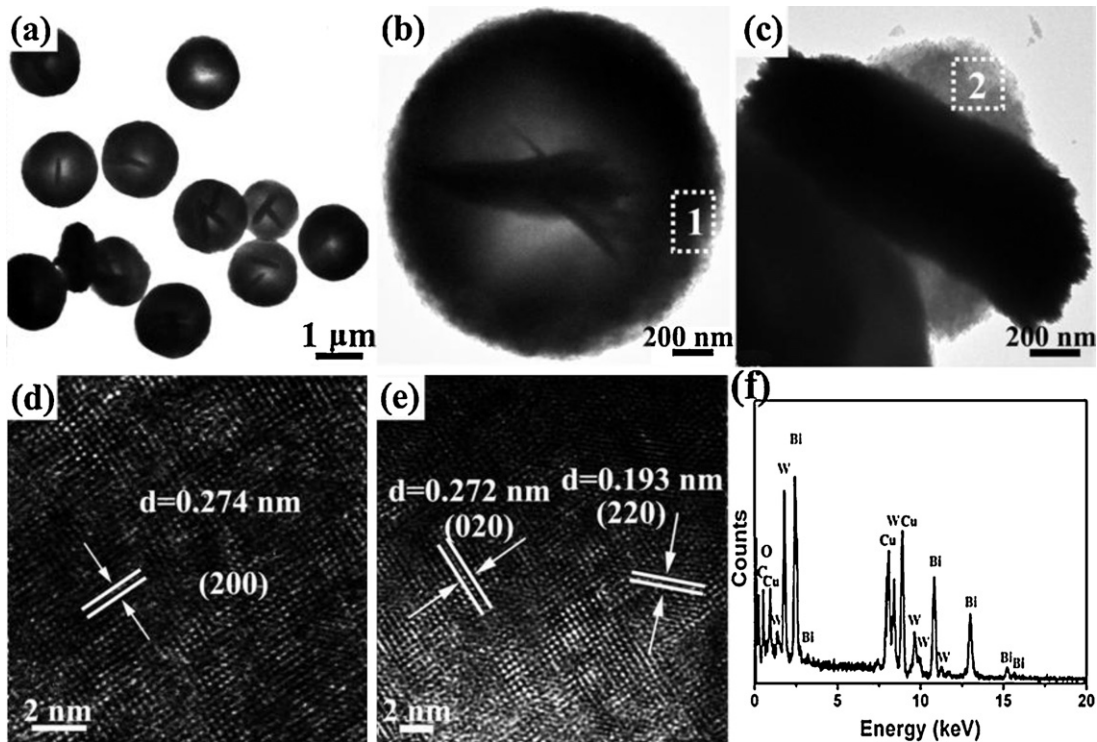

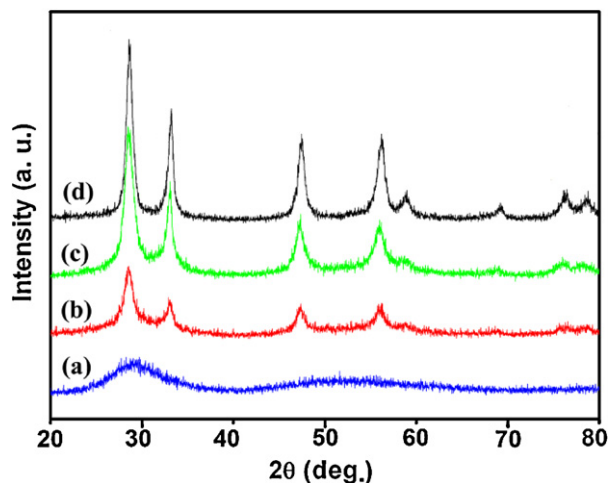**Fig. 4.** (a–c) Typical TEM and (d and e) HRTEM images of S-4. (f) The corresponding EDX pattern.

Fig. 5. XRD patterns of four samples: (a) S-1, (b) S-2, (c) S-3, (d) S-4.

Fig. 6. Responses of four sensors to 50 ppm ethanol at different operating temperatures.

(2 2 0) of orthorhombic Bi_2WO_6, respectively. EDX spectroscopy (Fig. 4f) displays that the S-4 are elementally composed of Bi, W, and O. The signal of Cu originates from the copper grid, and no other elements are detected.

The corresponding XRD patterns of the time-dependent products are shown in Fig. 5, and the crystallinity of the products increased with increasing reaction time. The XRD patterns of the products obtained from S-1 to S-4 are well indexed to Bi_2WO_6 (JCPDS No. 73-1126). XRD pattern of the products obtained before solvothermal reaction-treatment reveals it is amorphous (Fig. 5a). When the solvothermal reaction time is prolonged to 10 min (S-2) or longer (S-3, S-4), the diffraction peaks become gradually stronger in relative intensity, demonstrating that the crystallinity of the product improved significantly with the reaction time increased (Fig. 5b–d). Moreover, we can conclude that the crystallite sizes of the samples S-2, S-3 and S-4 increased with decreasing the width of the main peaks.

3.2. Gas-sensing properties

To demonstrate the usage of such unique nanomaterials, four gas sensors have been fabricated from the synthesized Bi_2WO_6 samples and investigated for ethanol detection. The working temperature range is an important functional characteristic for semiconductor oxide sensors. Fig. 6 shows the responses of four sensors to 50 ppm of ethanol at operating temperatures from 240 to 360 °C. The sensors show different responses with the operating temperature changed and the highest responses of each sensor are also different. The highest response is obtained at the operating temperature of 280 °C for the S-4 sensor. It is worthy to note that the operating temperature has a slight shift in the maximum response toward lower temperatures with the crystallinity increased. As an optimum between response/recovery time and the response, the operating temperatures of 280 °C (S-3, S-4) and 300 °C (S-1, S-2) are chosen for the remainder of the experiments.

Response and response rate are two important factors of gas sensors: high response and fast response rate can usually allow for a low detection limit and a short detection time [10]. Fig. 7 presents the dynamic response-recovery curves of four sensors to different concentrations of ethanol. It can be seen that the response of S-4 sensor is much higher than that of other Bi_2WO_6. Furthermore, the S-4 sensor exhibits a fast response time (1 s) to ethanol. However, the response times of the S-1–S-3 sensors are much longer than that of the S-4. The remarkable response and fast response rate can be attributed to the uniquely structures with the high surface area and
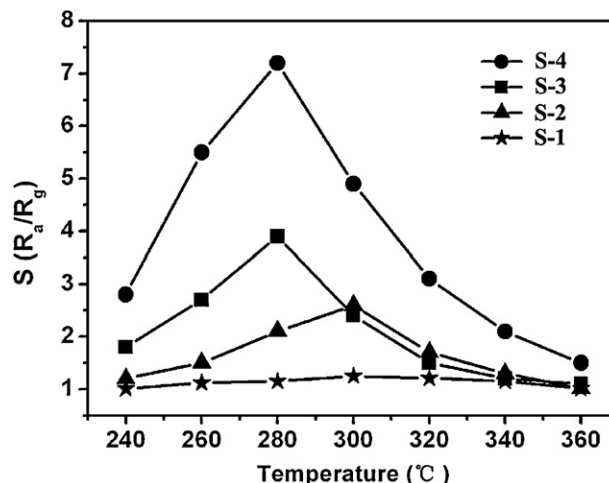
the rapid diffusion of the target gas toward their sensing surface via well-aligned nanostructures. It can be observed (in Fig. 4c) that the surfaces of the curling-like structure are very rough and loose. Thus, the gas diffusion toward the entire sensing surface is not hampered, which exhibits a fast response/recovery time [23,24]. The inset of Fig. 7 shows the resistance-temperature behavior in air of Bi_2WO_6 sensors. Over the whole temperature range studied, the resistance values of all the sensors decrease with increasing working temperature due to the intrinsic characteristics of the semiconductor.

We then investigated the response of these sensors at different ethanol concentrations (Fig. 8). Fig. 8a shows the response of S-4 sensor increased rapidly with further increases in ethanol concentration from 10 to 300 ppm, but increased more slowly from 800 to 2000 ppm as the sensor began to saturate. The responses of S-4 sensor to 10–2000 ppm ethanol ranged from 3.0 to 29.8, which was about 2–13 times higher than that of other Bi_2WO_6 sensor. Fig. 8b shows that the increase in the responses depends nearly linear on the gas concentrations in the range from 10 to 100 ppm for four sensors, which further confirms that the S-4 are more favorable to detect ethanol with low concentration. Fig. 9 depicts the histogram of the response of four sensors to 50 ppm of various gas vapors, including ethanol, acetone, ammonia, methanol and
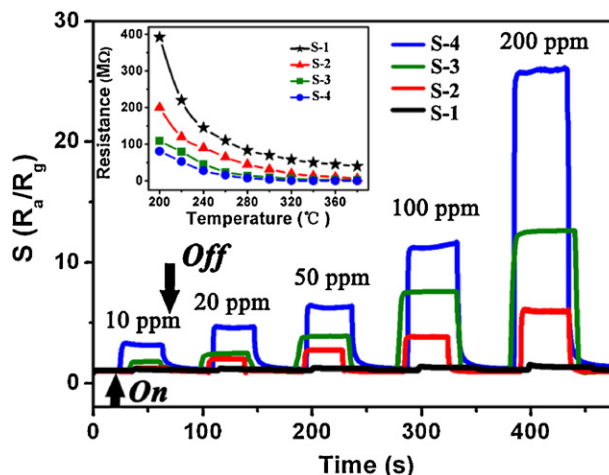

Fig. 7. Dynamic ethanol sensing transients for the sensors composed of S-1 (300 °C), S-2 (300 °C), S-3 (280 °C) and S-4 (280 °C). The insets show the relationship between the resistance in air and the working temperature of sensor components with the S-1, S-2, S-3 and S-4, respectively.
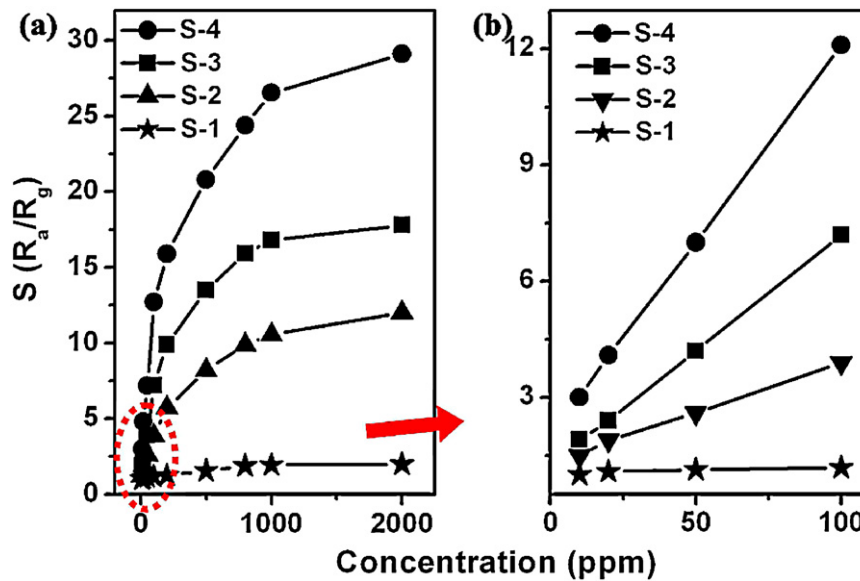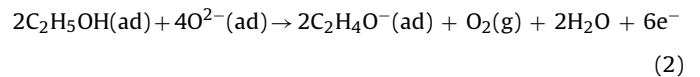
Fig. 8. Comparison in sensor response to different concentrations of ethanol for Bi_2WO_6 prepared with different reaction times versus: (a) high concentration and (b) low concentration.

toluene. Clearly, the responses of S-4 sensor to five gases are all improved compared with the others, and the largest increase is only observed for ethanol, implying the good selectivity of the sensor for ethanol.

The gas-sensing property of S-4 sensor for ethanol is much better than that of others. This may be attributed to two factors. One is that S-4 exhibits good crystallization. It can be observed (in Fig. 5) that the crystallinity of the products was improved as the reaction time was prolonged. It is well known that the crystallization is the most important parameters to enhance the gas sensing performances [25]. The other factor is their unique structure assembled by the nanosheets, resulting in a much larger surface area and well-aligned nanostructures which have been demonstrated by Brunauer–Emmett–Teller (BET) method (Table 1). The response of metal oxide gas sensors is based on the adsorption and desorption, the exchange of charges between absorbed gaseous species and the metal oxide surface. In the air, oxygen molecules are adsorbed onto S-4 sample to form chemisorbed oxygen species (O^-, O^{2-}) by capturing free electrons from the conduction band. Thus, a depletion layer at S-4 surface is formed. When the S-4 is exposed to target gas, the ethanol molecules will react with the adsorbed oxygen species

on the surface and release the trapped electrons back to the conduction band leads to the increase of conductivity, as in Eqs. (1) and (2) [26].

$$C_2H_5OH(g) \rightarrow C_2H_5OH(ad) \tag{1}$$

$$2C_2H_5OH(ad) + 4O^{2-}(ad) \rightarrow 2C_2H_4O^-(ad) + O_2(g) + 2H_2O + 6e^- \tag{2}$$

4. Conclusion

In summary, nanoparticles, nanosheets, compact nanosheets and curling-like Bi_2WO_6 structures were fabricated as gas sensors and their ethanol sensing characteristics were also investigated. The results reveal that curling-like Bi_2WO_6 sensor exhibits much higher response, faster response and recovery, and better selectivity than that of other products. Typically, the responses for curling-like Bi_2WO_6 structure to 50 ppm ethanol were about 2–5 times compared to other structures. The response and recovery times for curling-like Bi_2WO_6 are about 1 and 7 s, respectively, implying that curling-like Bi_2WO_6 is suitable for fabricating ethanol sensor.

Fig. 9. Responses to 50 ppm of different gases for sensors composed of Bi_2WO_6 prepared with different reaction times.

References

[1] Z.L. Wang, J.H. Song, Piezoelectric nanogenerators based on zinc oxide nanowire arrays, Science 312 (2006) 242–246.
[2] X.L. Li, W.J. Wei, S.Z. Wang, L. Kuai, B.Y. Geng, Single-crystalline α-Fe₂O₃ oblique nanoparallelepipeds: high-yield synthesis, growth mechanism and structure enhanced gas-sensing properties, Nanoscale 3 (2011) 718–724.
[3] B.X. Li, Y. Xie, M. Jing, G.X. Rong, Y.C. Tang, G.Z. Zhang, In₂O₃ hollow microspheres: synthesis from designed In(OH)₃ precursors and applications in gas sensors and photocatalysis, Langmuir 22 (2006) 9380–9385.

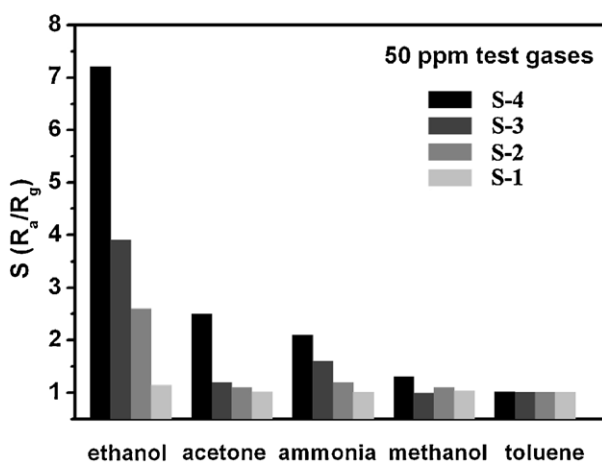[4] M. Niederberger, H. Colfen, Oriented attachment and mesocrystals: non-classical crystallization mechanisms based on nanoparticle assembly, Physical Chemistry Chemical Physics 8 (2006) 3271–3287.

[5] J. Wu, F. Duan, Y. Zheng, Y.J. Xie, Synthesis of Bi_2WO_6 nanoplate-built hierarchical nest-like structures with visible-light-induced photocatalytic activity, Journal of Physical Chemistry C 111 (2007) 12866–12871.

[6] X.B. Cao, L. Gu, L.J. Zhuge, W.J. Gao, W.C. Wang, S.F. Wu, Template-free preparation of hollow Sb_2S_3 microspheres as supports for Ag nanoparticles and photocatalytic properties of the constructed metal-semiconductor nanostructures, Advanced Functional Materials 16 (2006) 896–902.

[7] Q.R. Zhao, Y.G.X. Bai, Optimisation of the electrochemical bath for growing device-quality $CuInSe_2$ thin films, European Journal of Inorganic Chemistry 8 (2006) 1643–1649.

[8] L.L. Wang, Z. Lou, T. Zhang, H.T. Fan, X.J. Xu, Facile synthesis of hierarchical SnO_2 semiconductor microspheres for gas sensor application, Sensors and Actuators B 155 (2011) 285–289.

[9] S. Ashraf, C.S. Blackman, R.G. Palgrave, S.C. Naisbitt, I.P. Parkin, Aerosol assisted chemical vapour deposition of WO_3 thin films from tungsten hexacarbonyl and their gas sensing properties, Journal of Materials Chemistry 17 (2007) 3708–3713.

[10] L.L. Wang, Z. Lou, T. Fei, T. Zhang, Zinc oxide core–shell hollow microspheres with multi-shelled architecture for gas sensor applications, Journal of Materials Chemistry 21 (2011) 19331–19336.

[11] Y.F. Cui, C. Wang, S.J. Wu, G. Liu, F.F. Zhang, T.M. Wang, Lotus-root-like NiO nanosheets and flower-like NiO microspheres: synthesis and magnetic properties, CrystEngComm 13 (2011) 4930–4934.

[12] J.Y. Liu, T. Luo, F.L. Meng, K. Qian, Y.T. Wan, J.H. Liu, Porous hierarchical In_2O_3 micro-/nanostructures: preparation, formation mechanism, and their application in gas sensors for noxious volatile organic compound detection, Journal of Physical Chemistry C 114 (2010) 4887–4894.

[13] S.Y. Bae, J. Lee, H. Jung, J. Park, J.P. Ahn, Helical structure of single-crystalline $ZnGa_2O_4$ nanowires, Journal of the American Chemical Society 127 (2005) 10802–10803.

[14] J. Wu, F. Duan, Y. Zheng, Y. Xie, Synthesis of Bi_2WO_6 nanoplate-built hierarchical nest-like structures with visible-light-induced photocatalytic activity, Journal of Physical Chemistry C 111 (2007) 12866–12871.

[15] W. Qu, W. Wlodarski, J.U. Meyer, Comparative study on micromorphology and humidity sensitive properties of thin-film and thick-film humidity sensors based on semiconducting $MnWO_4$, Sensors and Actuators B 64 (2000) 76–82.

[16] S.H. Yu, B. Liu, M.-S. Mo, J.H. Huang, X.M. Liu, Y.T. Qian, General synthesis of single-crystal tungstate nanorods/nanowires: a facile, low-temperature solution approach, Advanced Functional Materials 13 (2003) 639–647.

[17] S. Driscoll, U.S. Ozkan, Isotopic labeling studies on oxidative coupling of methane over alkali promoted molybdate catalysts, Studies in Surface Science and Catalysis 82 (1994) 367–375.

[18] Y. Zhou, Z.P. Tian, Z.Y. Zhao, Q. Liu, J.H. Kou, X.Y. Chen, J. Gao, S.C. Yan, Z.G. Zou, High-yield synthesis of ultrathin and uniform Bi_2WO_6 square nanoplates benefitting from photocatalytic reduction of CO_2 into renewable hydrocarbon fuel under visible light, ACS Applied Materials & Interfaces 3 (2011) 3594–3601.

[19] L.S. Zhang, W.Z. Wang, L. Zhou, H.L. Xu, Bi_2WO_6 nano- and microstructures: shape control and associated visible-light-driven photocatalytic activities, Small 3 (2007) 1618–1625.

[20] X.J. Dai, Y.S. Luo, W.D. Zhang, S.Y. Fu, Facile hydrothermal synthesis and photocatalytic activity of bismuth tungstate hierarchical hollow spheres with an ultrahigh surface area, Dalton Transactions 39 (2010) 3426–3432.

[21] L.S. Zhang, W.Z. Wang, Z.J. Chen, L. Zhou, H.L. Xu, W. Zhu, Fabrication of flower-like Bi_2WO_6 superstructures as high performance visible-light driven photocatalysts, Journal of Materials Chemistry 17 (2007) 2526–2532.

[22] K.B. Zheng, Y. Zhou, L.L. Gu, X.L. Mo, G.R. Patzke, G.R. Chen, Humidity sensors based on Aurivillius type Bi_2MO_6 (M = W, Mo) oxide films, Sensors and Actuators B 148 (2010) 240–246.

[23] T. Hyodo, N. Nishida, Y. Shimizu, M. Egashira, Preparation and gas-sensing properties of thermally stable mesoporous SnO_2, Sensors and Actuators B 83 (2002) 209–215.

[24] J.H. Lee, Gas sensors using hierarchical and hollow oxide nanostructures: overview, Sensors and Actuators B 140 (2009) 319–336.

[25] A. Gurlo, Nanosensors: towards morphological control of gas sensing activity. SnO_2, In_2O_3, ZnO and WO_3 case studies, Nanoscale 3 (2011) 154–165.

[26] J. Zhang, S.R. Wang, Y. Wang, M.J. Xu, H.j. Xia, S.M. Zhang, W.P. Huang, X.Z. Guo, S.H. Wu, Facile synthesis of highly ethanol-sensitive SnO_2 nanoparticles, Sensors and Actuators B 139 (2009) 369–374.

Biographies

Zheng Lou received his BS degree from the College of Electronics Science and Engineering, Jilin University, China in 2009. As an MS student, his research interest is gas sensors based on semiconducting functional materials.

Jianan Deng received his BS degree from the College of Electronics Science and Engineering, Jilin University, China in 2011. As an MS student, his research interest is gas sensors based on semiconducting functional materials.

Lili Wang received her MS degree in Chemistry from Jilin University, China in 2010. She entered the PhD course in 2010, majoring in microelectronics and solid-state electronics. She is studying the synthesis and characterization of semiconducting, functional materials and gas sensors.

Lijie Wang received her MS and Dr degree from the College of Electronics Science and Engineering, Jilin University, China in 2005 and 2010, respectively. She majored in microelectronics and solid state electronics, and engaged in IC design.

Tong Zhang completed her MS degree in semiconductor materials in 1992 and her PhD in the field of microelectronics and solid-state electronics in 2001 from Jilin University. She was appointed as a full-time professor in the College of Electronics Science and Engineering, Jilin University in 2001. Her research interests are sensing functional materials, gas sensors, and humidity sensors.